Conference Proceedings of the Society for Experimental Mechanics Series

R. Mayes · D. Rixen · D.T. Griffith · D. De Klerk · S. Chauhan
S.N. Voormeeren · M.S. Allen *Editors*

Topics in Experimental Dynamics Substructuring and Wind Turbine Dynamics, Volume 2

Proceedings of the 30th IMAC, A Conference on Structural Dynamics, 2012

SEM Springer

Conference Proceedings of the Society for Experimental Mechanics Series

Series Editor
Tom Proulx
Society for Experimental Mechanics, Inc.,
Bethel, CT, USA

For further volumes:
http://www.springer.com/series/8922

R. Mayes • D. Rixen • D.T. Griffith • D. De Klerk
S. Chauhan • S.N. Voormeeren • M.S. Allen
Editors

Topics in Experimental Dynamics Substructuring and Wind Turbine Dynamics, Volume 2

Proceedings of the 30th IMAC, A Conference on Structural Dynamics, 2012

Springer

Editors
R. Mayes
Sandia National Laboratories
Albuquerque, NM, USA

D.T. Griffith
Sandia National Laboratories
Albuquerque, NM, USA

S. Chauhan
Brüel and Kjær
Skodsborgvej, Denmark

M.S. Allen
University of Wisconsin
Madison, WI, USA

D. Rixen
Delft University of Technology
The Netherlands

D. De Klerk
Delft University of Technology
The Netherlands

S.N. Voormeeren
Delft University of Technology
The Netherlands

ISSN 2191-5644 e-ISSN 2191-5652
ISBN 978-1-4614-2421-5 e-ISBN 978-1-4614-2422-2
DOI 10.1007/978-1-4614-2422-2
Springer New York Dordrecht Heidelberg London

Library of Congress Control Number: 2012936658

Preface

Topics in Experimental Dynamics Substructuring and Wind Turbine Dynamics represents one of six volumes of technical papers presented at the 30th IMAC, A Conference and Exposition on Structural Dynamics, 2012 organized by the Society for Experimental Mechanics, and held in Jacksonville, Florida, January 30 – February 2, 2012. The full proceedings also include volumes on Dynamics of Civil Structures; Nonlinear Dynamics; Model Validation and Uncertainty Quantification; and Modal Analysis, I & II.

Each collection presents early findings from experimental and computational investigations on an important area within Structural Dynamics. The current volume on *Topics in Experimental Dynamics Substructuring and Wind Turbine Dynamics* presents research in two areas of great importance. Recent advances in experimental techniques, sensor/actuator technologies, novel numerical methods, and parallel computing have rekindled interest in substructuring in recent years leading to new insights and improved experimental and analytical techniques.

Governments around the world have set ambitious goals of meeting 20% of energy requirements by 2020 through renewable energy sources including wind energy. This presents challenges, including the growing size and complexity of the wind turbine structure, necessitating the need for designers to better understand and characterize the dynamics of the wind turbine. Despite well-established techniques (Experimental and Operational Modal Analysis) for dynamic characterization of structures, their application to wind turbines is not straight forward due to the complexities involved on account of considerable aeroelastic interaction and time-varying nature of wind turbines, when in operation. This volume showcases research activities with regards to application of modal analysis to wind turbines, preparing and updating numerical models, instrumentation and sensing on wind turbine blades, and structural health monitoring as applied to wind turbines.

The organizers would like to thank the authors, presenters, session organizers, and session chairs for their participation in this track.

Albuquerque, NM, USA — R. Mayes
The Netherlands — D. Rixen
Albuquerque, NM, USA — D.T. Griffith
The Netherlands — D. De Klerk
Skodsborgvej, Denmark — S. Chauhan
The Netherlands — S.N. Voormeeren
Madison, WI, USA — M.S. Allen

Contents

Chapter 1
Tutorial on Experimental Dynamic Substructuring Using the Transmission Simulator Method*

Randy L. Mayes

Abstract Although analytical substructures have been used successfully for years, practical experimental substructures have been limited to special cases until recently. Many of the historical practical applications were based on a single point attachment. Since substructures have to be connected, theoretically, in both translation and rotation degrees of freedom, measurement translation responses and forces around the single point attachment could be used to estimate the rotational responses and moments. For multiple attachment points, often the rotations and moments have been neglected entirely. In addition, often the effect of the joint stiffness and damping is neglected. The translation simulator approach developed by Allen and Mayes captures the interface forces and motions through a fixture called the transmission simulator, overcoming the historical difficulties. The experimental free modes of the experimental substructure mounted to the transmission simulator and the finite element model of the transmission simulator are used to couple the experimental substructure to another substructure and subtract the transmission simulator. This captures the effects of the joint stiffness and damping. The experimental method and mathematics will be explained with examples. The tutorial assumes a basic understanding of the linear multi-degree of freedom equations of motion and the modal approximation.

1.1 Introduction

The modal constraint for fixture and subsystem (MCFS) method was introduced at IMAC in 2007 for the component mode synthesis approach (Allen and Mayes [1]) and the Frequency Based Substructuring approach (Mayes and Stasiunas [2]). It uses a fixture in the experimental dynamic substructure called the transmission simulator, so is also called the transmission simulator method. An analytical model of the transmission simulator is always required with this method.

Physically, the transmission simulator is mounted to the experimental substructure with exactly the same joint geometry and material as that to which the experimental substructure will ultimately be connected. Because of this, the resulting experimental substructure inherently includes the linearized stiffness and damping in the joint, which classical methods neglect, to their peril. The fixture is also designed to provide accessible locations to mount response sensors and to apply input forces. Often the actual connection points are poor locations to mount sensors. For example, the connection point may be at a bolt or a threaded screw interface. Special features can also be included to provide good driving point measurements, which are extremely important to obtain accurate modal mass for scaling the mode shapes.

The analytical model of the transmission simulator is used in multiple ways. It is generally mounted with an assumed welded connection to the analytical substructure (often a finite element model) to which the experimental substructure is to be connected. By constraining the transmission simulator on the experimental substructure to have the same motion as the transmission simulator on the analytical substructure, the systems are joined. Then the mass and stiffness of the analytical and experimental transmission simulators are subtracted from the assembled system. The analytical model of the transmission simulator can also be thought of as an aid to interpolate from the measurement sensor locations back to the actual

*Sandia is a multi-program laboratory operated by Sandia Corporation, a Lockheed Martin Company, for the United States Department of Energy's National Nuclear Security Administration under Contract DE-AC04-94AL85000.

R.L. Mayes (✉)
Experimental Mechanics, NDE and Model Validation Department, Sandia National Laboratories,
5800 – MS0557, Albuquerque, NM 87185, USA
e-mail: rlmayes@sandia.gov

R.L. Mayes et al. (eds.), *Topics in Experimental Dynamics Substructuring and Wind Turbine Dynamics, Volume 2*,
Conference Proceedings of the Society for Experimental Mechanics Series 27,
DOI 10.1007/978-1-4614-2422-2_1,

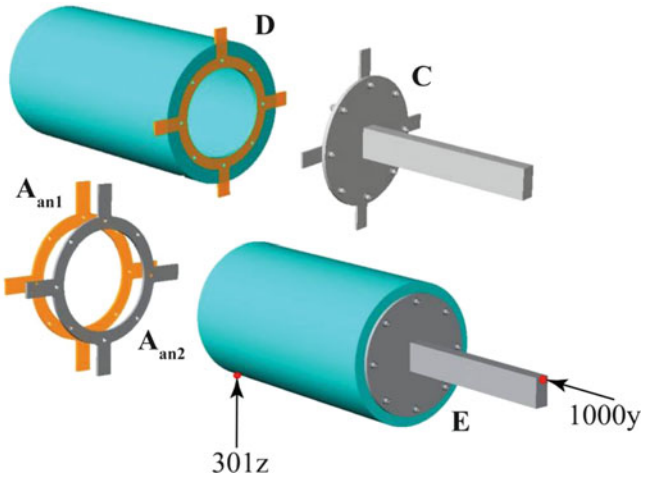

Fig. 1.1 Coupling of experimental substructure C with analytical substructure D to generate full system E after transmission simulators (A_{an1} and A_{an2}) are subtracted

connection degrees of freedom (dof). A truncated set of the mode shapes of the transmission simulator is used that spans the frequency bandwidth of interest. The sensor set can be chosen to provide a set of sensor locations for which all chosen transmission shapes are linearly independent. These sensors can all be translational – no rotations are required. The rotations at the connection points are inherently carried in the modal coordinates of the transmission simulator. The connections can actually be continuous, not just discrete, as long as the transmission simulator mode shape set spans the space of the connection motion reasonably well. In addition the transmission simulator mass stresses the joint. This stress across the joint provides a much better Ritz vector shape basis than simple free modes where there is no stress at the joint. It provides enough improvement in the basis vectors that residuals, which are difficult to measure, do not need to be added to the basis set.

Although this method requires fabrication of a fixture and generation of its associated analytical model, it provides extensive benefits for the investment. One does not have to measure exactly at the connection points. One does not have to measure rotations because they are inherently included in the analytical model modal coordinates (so they are not just being neglected). The stiffness and damping of the joint are inherently included. No residual measurements are required.

One problem that can result in this method is that the mass matrix can be indefinite when the transmission simulator is subtracted. However, methods to correct the mass matrix have been developed recently [3]. This has cleared the way so that in practice, refinements can be made without theoretical road blocks.

An example from [3] shows conceptually how the method was implemented for one actual hardware case in Fig. 1.1. The transmission simulator hardware, which is a ring with tabs, is mounted to the experimental substructure with eight bolts, just as it will be attached in the real system to the cylinder substructure, so it contains the joint. An analytical model of the transmission simulator is welded in to the flange of the cylinder analytical model. The transmission simulator and the cylinder flange actually occupy the same space, which can be done with an analytical model. Then transmission simulators for each substructure are forced to have the same motion, which connects them. Finally the stiffness and mass of the two transmission simulators are analytically subtracted.

The free-free experimental modal test setup is shown in Fig. 1.2 with 12 triaxial accels on the transmission simulator and 2 triaxial accels at points of interest on the beam. Twenty five rigid body and elastic modes were extracted out to 4 kHz. This structure had eight discrete bolted attachments, which would require 48 discrete constraints for the three rotations and three translations at each connection. Figure 1.3 shows the 12 triax locations, which are not at the eight connection points. 18 modes of the transmission simulator analytical model were used to span the connection space motion, using 36 measured dof to describe the mode shapes. The method thus reduces the number of constraints down from the classic 48 connections to 18. The 18 modes covered a frequency bandwidth of 2 kHz.

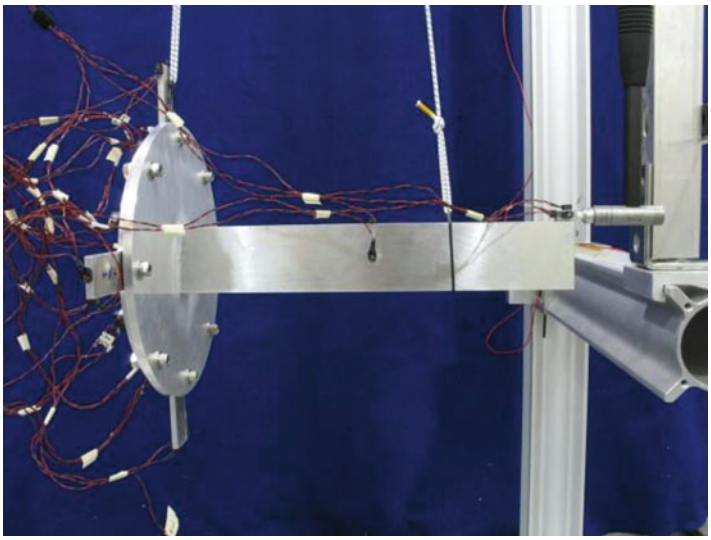

Fig. 1.2 Experimental substructure free modal test setup with 36 sensors on the transmission simulator ring and a few sensors at points of interest on the substructure

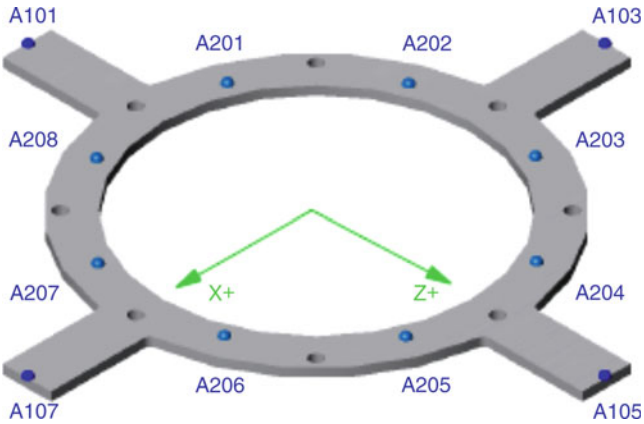

Fig. 1.3 Transmission simulator with 12 triaxial accelerometers at blue nodes for sensing

1.2 Component Mode Synthesis Theory Using Primal Formulation in a Generalized Framework

The generalized framework of deKlerk, Rixen and Voormeeren [4] for dynamic substructuring is utilized. Here assume that each substructure has been approximated with a reduced model, whether experimental or analytical. Then the displacements are approximated with the modal substitution as

$$\bar{\mathbf{u}} \cong \mathbf{R}\bar{\boldsymbol{\eta}} \tag{1.1}$$

where $\bar{\mathbf{u}}$ is the vector of physical displacements, $\bar{\boldsymbol{\eta}}$ is the vector of generalized coordinates from a modal test or eigenvector analysis and $\mathbf{R}$ is the truncated mode shape matrix relating the generalized coordinates to the physical coordinates. Then the equations of motion for the substructure can be written as

$$\mathbf{M}^{(s)}\mathbf{R}\ddot{\bar{\boldsymbol{\eta}}}^{(s)} + \mathbf{C}^{(s)}\mathbf{R}\dot{\bar{\boldsymbol{\eta}}}^{(s)} + \mathbf{K}^{(s)}\mathbf{R}\bar{\boldsymbol{\eta}}^{(s)} = \bar{\mathbf{f}}^{(s)} + \bar{\mathbf{g}}^{(s)} + \bar{\mathbf{r}}^{(s)} \tag{1.2}$$

Where $\mathbf{M}$, $\mathbf{C}$ and $\mathbf{K}$ are mass stiffness and damping matrices, the superscript *(s)* denotes the particular substructure, $\bar{\mathbf{f}}^{(s)}$ denotes the external forces applied to the substructure, $\bar{\mathbf{g}}^{(s)}$represents the equilibrium joining forces from another substructure

that will be applied to the substructure, and $\bar{\mathbf{r}}^{(s)}$is the residual force due to the mismatch caused by the approximation of the displacements in (1.1). Premultiplying by $\mathbf{R}^T$ yields

$$\mathbf{R}^T\mathbf{M}^{(s)}\mathbf{R}\ddot{\bar{\boldsymbol{\eta}}}^{(s)} + \mathbf{R}^T\mathbf{C}^{(s)}\mathbf{R}\dot{\bar{\boldsymbol{\eta}}}^{(s)} + \mathbf{R}^T\mathbf{K}^{(s)}\mathbf{R}\bar{\boldsymbol{\eta}}^{(s)} = \mathbf{R}^T\bar{\mathbf{f}}^{(s)} + \mathbf{R}^T\bar{\mathbf{g}}^{(s)} + \mathbf{R}^T\bar{\mathbf{r}}^{(s)}. \tag{1.3}$$

It can be shown that, because of orthogonality of the mode shapes with respect to **M**, **C** and **K**,

$$\mathbf{R}^T\bar{\mathbf{r}}^{(s)} = \bar{\mathbf{0}} \tag{1.4}$$

which leaves

$$\mathbf{R}^T\mathbf{M}^{(s)}\mathbf{R}\ddot{\bar{\boldsymbol{\eta}}}^{(s)} + \mathbf{R}^T\mathbf{C}^{(s)}\mathbf{R}\dot{\bar{\boldsymbol{\eta}}}^{(s)} + \mathbf{R}^T\mathbf{K}^{(s)}\mathbf{R}\bar{\boldsymbol{\eta}}^{(s)} = \mathbf{R}^T\bar{\mathbf{f}}^{(s)} + \mathbf{R}^T\bar{\mathbf{g}}^{(s)}, \tag{1.5}$$

or in a renamed form

$$\mathbf{M}_m^{(s)}\ddot{\bar{\boldsymbol{\eta}}}^{(s)} + \mathbf{C}_m^{(s)}\dot{\bar{\boldsymbol{\eta}}}^{(s)} + \mathbf{K}_m^{(s)}\bar{\boldsymbol{\eta}}^{(s)} = \bar{\mathbf{f}}_m^{(s)} + \bar{\mathbf{g}}_m^{(s)} \tag{1.6}$$

where subscript m denotes modal quantities. The matrices are, if the mode shapes are mass normalized,

$$\begin{aligned}
\mathbf{M}_m^{(s)} &= \mathbf{R}^T\mathbf{M}^{(s)}\mathbf{R} = \mathbf{I} \\
\mathbf{C}_m^{(s)} &= \mathbf{R}^T\mathbf{C}^{(s)}\mathbf{R} = diag(2^*\bar{\boldsymbol{\zeta}}.^*\bar{\boldsymbol{\omega}}) \\
\mathbf{K}_m^{(s)} &= \mathbf{R}^T\mathbf{K}^{(s)}\mathbf{R} = diag(\bar{\boldsymbol{\omega}}.\hat{}2) \\
\bar{\mathbf{f}}_m^{(s)} &= \mathbf{R}^T\mathbf{f}^{(s)} \\
\bar{\mathbf{g}}_m^{(s)} &= \mathbf{R}^T\mathbf{g}^{(s)}.
\end{aligned} \tag{1.7}$$

At this point, let us concatenate the various substructures together in the uncoupled form as

$$\mathbf{M}_m\ddot{\bar{\boldsymbol{\eta}}} + \mathbf{C}_m\dot{\bar{\boldsymbol{\eta}}} + \mathbf{K}_m\bar{\boldsymbol{\eta}} = \bar{\mathbf{f}}_m + \bar{\mathbf{g}}_m. \tag{1.8}$$

Compatibility is now enforced with a constraint equation from

$$\mathbf{B}\bar{\mathbf{u}}_c = \bar{\mathbf{0}} \tag{1.9}$$

Where **B** is a Boolean matrix of ones, zeros and negative ones, and for convenience we will include only connection dof in the displacement vector. Take the partition of (1.1) for only the connection dof and again make the modal substitution

$$\mathbf{B}\mathbf{R}_c\bar{\boldsymbol{\eta}} \cong \bar{\mathbf{0}} \tag{1.10}$$

where the subscript c indicates taking only the partition of R necessary for the connection dof.

Up to this point we have followed the generalized framework rather strictly, but at this point, the transmission simulator method affects the rest of the development. It is assumed that there is an analytical model of the transmission simulator, one uses a truncated set of its mode shapes, Ψ_c, as a basis to span the space of the connection motion for each substructure. Now we use the pseudo-inverse (denoted with a superscript +) to project the constraint on the space of the transmission simulator vector space by premultiplying both sides by the block diagonal pseudo-inverse as

$$\Psi_c^{BD+}\mathbf{B}\mathbf{R}_c\bar{\boldsymbol{\eta}} \cong \Psi_c^{BD+}\bar{\mathbf{0}} \tag{1.11}$$

where

$$\Psi_c^{BD+} = \begin{bmatrix} \Psi_c^+ & 0 & 0 \\ 0 & \ldots & 0 \\ 0 & 0 & \Psi_c^+ \end{bmatrix} \tag{1.12}$$

will have as many block rows as there are substructures. The right hand side of (1.11) is still a vector of zeros, although the number of constraints (rows) is reduced since the matrix $\Psi_c$is selected so that it always has more dof than modes. The final constraint is

$$\tilde{\mathbf{B}}\bar{\boldsymbol{\eta}} = \bar{\mathbf{0}} \tag{1.13}$$

where

$$\tilde{\mathbf{B}} = \Psi_c^{BD+}\mathbf{B}\mathbf{R}_c \tag{1.14}$$

There are multiple reasons for premultiplying by Ψ_c^{BD+}. First it softens the constraint (reduces the number of constraints). The advantage of this is that it gives a least squares fit through the measured motions of the transmission simulator at the dof to which the constraints will be applied. The mode shapes of the transmission simulator provide a smoothing effect through the measured motions, which always have experimental error. The modified matrix greatly improves the conditioning of the problem. Also, one does not HAVE to use motions measured directly at the attachment points and also does not HAVE to measure rotations, which are inherently carried along in the generalized dof of the transmission simulator. The generalized modal dof of the transmission simulator are $\bar{\boldsymbol{\gamma}}$ in the following

$$\Psi_c\bar{\boldsymbol{\gamma}} \cong \mathbf{R}_c^{(s)}\bar{\boldsymbol{\eta}}^{(s)} \tag{1.15}$$

but can be expressed as

$$\bar{\boldsymbol{\gamma}} \cong \Psi_c^{+}\mathbf{R}_c^{(s)}\bar{\boldsymbol{\eta}}^{(s)} \tag{1.16}$$

which can be seen in the left hand side of (1.11) as converting the constraint to the transmission simulator modal coordinates.

Now continue the development in the general framework from (1.13). We perform another modal-like substitution with

$$\bar{\boldsymbol{\eta}} = \tilde{\mathbf{L}}\bar{\boldsymbol{\varepsilon}}. \tag{1.17}$$

Substitute (1.17) into (1.13) to give

$$\tilde{\mathbf{B}}\tilde{\mathbf{L}}\bar{\boldsymbol{\varepsilon}} = \bar{\mathbf{0}}. \tag{1.18}$$

If one chooses $\tilde{\mathbf{L}}$ such that it is in the null space of $\tilde{\mathbf{B}}$, then (1.18) is guaranteed to be satisfied because

$$\tilde{\mathbf{B}}\tilde{\mathbf{L}} = [zeros]. \tag{1.19}$$

All the rows of $\tilde{\mathbf{B}}$ are orthogonal to all the columns of $\tilde{\mathbf{L}}$. Since $\tilde{\mathbf{B}}$ is known, a one line command in matlab can provide $\tilde{\mathbf{L}}$. Substituting (1.17) back into the uncoupled equations of motion in (1.8) and premultiplying by $\tilde{\mathbf{L}}^T$ gives

$$\tilde{\mathbf{L}}^T\mathbf{M}_m\tilde{\mathbf{L}}\ddot{\bar{\boldsymbol{\varepsilon}}} + \tilde{\mathbf{L}}^T\mathbf{C}_m\tilde{\mathbf{L}}\dot{\bar{\boldsymbol{\varepsilon}}} + \tilde{\mathbf{L}}^T\mathbf{K}_m\tilde{\mathbf{L}}\bar{\boldsymbol{\varepsilon}} = \tilde{\mathbf{L}}^T\bar{\mathbf{f}}_m + \tilde{\mathbf{L}}^T\bar{\mathbf{g}}_m, \tag{1.20}$$

which couples the equations of motion, reducing the number of rows in (1.8) by the number of constraints (rows) in (1.13). This leads to the primal coupling formulation in this framework. In this formulation $\tilde{\mathbf{L}}^T\bar{\mathbf{g}}_m = \tilde{\mathbf{L}}^T\mathbf{R}^T\bar{\mathbf{g}} = \bar{0}$, since the rows of $\tilde{\mathbf{L}}^T$ are orthogonal to a linear combination of the columns of $\mathbf{R}^T$, leaving

$$\tilde{\mathbf{M}}_m\ddot{\bar{\boldsymbol{\varepsilon}}} + \tilde{\mathbf{C}}_m\dot{\bar{\boldsymbol{\varepsilon}}} + \tilde{\mathbf{K}}_m\bar{\boldsymbol{\varepsilon}} = \tilde{\bar{\mathbf{f}}}_m \tag{1.21}$$

where

$$\begin{aligned}
\tilde{\mathbf{M}}_m &= \tilde{\mathbf{L}}^T\mathbf{M}_m\tilde{\mathbf{L}} \\
\tilde{\mathbf{C}}_m &= \tilde{\mathbf{L}}^T\mathbf{C}_m\tilde{\mathbf{L}} \\
\tilde{\mathbf{K}}_m &= \tilde{\mathbf{L}}^T\mathbf{K}_m\tilde{\mathbf{L}} \\
\tilde{\bar{\mathbf{f}}}_m &= \tilde{\mathbf{L}}^T\bar{\mathbf{f}}_m.
\end{aligned} \tag{1.22}$$

1.3 Frequency Based Substructuring Dual Formulation in the General Framework

Again following [4], for the physical dof, the uncoupled equations of motion, the compatibility and the equilibrium are written as

$$\mathbf{M}\ddot{\bar{\mathbf{u}}} + \mathbf{C}\dot{\bar{\mathbf{u}}} + \mathbf{K}\bar{\mathbf{u}} = \bar{\mathbf{f}} + \bar{\mathbf{g}} \tag{1.23}$$

$$\mathbf{B}\bar{\mathbf{u}} = \bar{\mathbf{0}} \tag{1.24}$$

$$\mathbf{L}^T\mathbf{g} = \bar{\mathbf{0}} \tag{1.25}$$

where $\mathbf{M}$, $\mathbf{C}$ and $\mathbf{K}$ are block diagonal with as many blocks as substructures. The constraint forces $\bar{\mathbf{g}}$ between the substructures can be written as

$$\mathbf{g} = -\mathbf{B}^T\bar{\boldsymbol{\lambda}} \tag{1.26}$$

where $\bar{\boldsymbol{\lambda}}$ are Lagrange multipliers corresponding physically to the interface forces. Equations (1.23) and (1.24) can now be written in matrix form as

$$\begin{bmatrix} \mathbf{M} & \mathbf{0} \\ \mathbf{0} & \mathbf{0} \end{bmatrix} \begin{bmatrix} \ddot{\mathbf{u}} \\ \boldsymbol{\lambda} \end{bmatrix} + \begin{bmatrix} \mathbf{C} & \mathbf{0} \\ \mathbf{0} & \mathbf{0} \end{bmatrix} \begin{bmatrix} \dot{\mathbf{u}} \\ \boldsymbol{\lambda} \end{bmatrix} + \begin{bmatrix} \mathbf{K} & \mathbf{B}^T \\ \mathbf{B} & \mathbf{0} \end{bmatrix} \begin{bmatrix} \mathbf{u} \\ \boldsymbol{\lambda} \end{bmatrix} = \begin{bmatrix} \mathbf{f} \\ \mathbf{0} \end{bmatrix}. \tag{1.27}$$

Taking the Fourier transform to put into the frequency domain, where each quantity is a function of frequency, gives

$$\begin{bmatrix} \mathbf{Z} & \mathbf{B}^T \\ \mathbf{B} & \mathbf{0} \end{bmatrix} \begin{bmatrix} \mathbf{u} \\ \boldsymbol{\lambda} \end{bmatrix} = \begin{bmatrix} \mathbf{f} \\ \mathbf{0} \end{bmatrix} \tag{1.28}$$

where $\mathbf{Z}$ is the block diagonal impedance matrix resulting from the mass, stiffness and damping. The frequency response function matrix, $\mathbf{H}$, which is often measured experimentally is the inverse of $\mathbf{Z}$. The dual formulation coupled formulation in terms of $\mathbf{H}$ is derived from (1.28) by eliminating $\boldsymbol{\lambda}$, yielding

$$\bar{\mathbf{u}} = \mathbf{H}\bar{\mathbf{f}} - \mathbf{H}\mathbf{B}^T(\mathbf{B}\mathbf{H}\mathbf{B}^T)^{-1}\mathbf{B}\mathbf{H}\bar{\mathbf{f}}. \tag{1.29}$$

The transmission simulator method modifies the $\mathbf{B}$ matrix in (1.24) as

$$\Psi^{BD+}\mathbf{B}\bar{\mathbf{u}} \cong \bar{\mathbf{0}} \tag{1.30}$$

So one has

$$\hat{\mathbf{B}}\bar{\mathbf{u}} = \bar{\mathbf{0}} \tag{1.31}$$

where

$$\hat{\mathbf{B}} = \Psi^{BD+}\mathbf{B}. \tag{1.32}$$

Now simply substitute (1.32) into (1.29) to give the frequency based transmission simulator equation as

$$\bar{\mathbf{u}} = \mathbf{H}\bar{\mathbf{f}} - \mathbf{H}\hat{\mathbf{B}}^T(\hat{\mathbf{B}}\mathbf{H}\hat{\mathbf{B}}^T)^{-1}\hat{\mathbf{B}}\mathbf{H}\bar{\mathbf{f}}. \tag{1.33}$$

The $\hat{\mathbf{B}}$ matrix transforms the physical connection dof frequency response functions (FRFs) into generalized dof FRFs cast on the space of the transmission simulator mode shapes. This collapses the size of the physical connection dof FRFs down to the size of the number of modes of the transmission simulator, providing some least squares smoothing, and makes the matrix inversion in (1.33) much better conditioned.

1.4 Example Combining Experimental Plate/Beam Substructure with Analytical Cylinder Substructure Using the CMS Approach

The example is based on the hardware and analytical finite element models depicted in the first three figures. In the equations below, the finite element (FE) substructure is considered to have the analytical model of the transmission simulator attached, and the experimental (EXP) substructure has the physical transmission simulator attached. Two transmission simulators must be subtracted. In this example, 100 modes were utilized from the finite element substructure, 25 modes from the experimental substructure, and 18 modes from the transmission simulator giving 143 uncoupled equations of motion. Consider only the eigenvalue equations of motion, and then the final coupled modal parameters can be used to analytically form any desired full system response FRF. Damping will be predicted in a simplified method later. The undamped frequency domain equations of motion using modal coordinates when forces are removed are

$$\begin{bmatrix} \boldsymbol{\omega}_{\mathbf{FE}}^2 & \mathbf{0} & \mathbf{0} \\ \mathbf{0} & \boldsymbol{\omega}_{\mathbf{EXP}}^2 & \mathbf{0} \\ \mathbf{0} & \mathbf{0} & -2\boldsymbol{\omega}_{\mathbf{TS}}^2 \end{bmatrix} \begin{Bmatrix} \boldsymbol{\eta}_{\mathbf{FE}} \\ \boldsymbol{\eta}_{\mathbf{EXP}} \\ \boldsymbol{\eta}_{\mathbf{TS}} \end{Bmatrix} - \omega^2 \begin{bmatrix} \mathbf{I}_{\mathbf{FE}} & \mathbf{0} & \mathbf{0} \\ \mathbf{0} & \mathbf{I}_{\mathbf{EXP}} & \mathbf{0} \\ \mathbf{0} & \mathbf{0} & -2\mathbf{I}_{\mathbf{TS}} \end{bmatrix} \begin{Bmatrix} \ddot{\boldsymbol{\eta}}_{\mathbf{FE}} \\ \ddot{\boldsymbol{\eta}}_{\mathbf{EXP}} \\ \ddot{\boldsymbol{\eta}}_{\mathbf{TS}} \end{Bmatrix} = \begin{Bmatrix} 0 \\ 0 \\ 0 \end{Bmatrix} \tag{1.34}$$

and the physical displacements, $\mathbf{y}$, on each substructures are

$$\begin{Bmatrix} \mathbf{y}_{\mathbf{FE}} \\ \mathbf{y}_{\mathbf{EXP}} \\ \mathbf{y}_{\mathbf{TS}} \end{Bmatrix} = \begin{bmatrix} \mathbf{R}_{\mathbf{FE}} & \mathbf{0} & \mathbf{0} \\ \mathbf{0} & \mathbf{R}_{\mathbf{EXP}} & \mathbf{0} \\ \mathbf{0} & \mathbf{0} & \mathbf{R}_{\mathbf{TS}} \end{bmatrix} \begin{Bmatrix} \boldsymbol{\eta}_{\mathbf{FE}} \\ \boldsymbol{\eta}_{\mathbf{EXP}} \\ \boldsymbol{\eta}_{\mathbf{TS}} \end{Bmatrix} \tag{1.35}$$

where $\mathbf{R}$ are a truncated set of the mass normalized mode shapes of each substructure coming from experiment or analysis. The motion of the transmission simulator in all three substructures should be the same when all the substructures are coupled, so two sets of physical constraints can be written

$$\mathbf{y}_{\mathrm{FEmeas}} = \mathbf{y}_{\mathrm{EXPmeas}} \text{ and } \mathbf{y}_{\mathrm{EXPmeas}} = \mathbf{y}_{\mathrm{TSmeas}} \tag{1.36}$$

Just consider the first of these constraints, invoke the modal substitution from (1.35) and premultiply by the pseudo-inverse of transmission simulator mode shapes, $\mathbf{R}_{\mathbf{TS}}^{+}$to give

$$\mathbf{R}_{\mathbf{TS}}^{+}\mathbf{R}_{\mathbf{FEmeas}}\bar{\boldsymbol{\eta}}_{\mathbf{FE}} = \mathbf{R}_{\mathbf{TS}}^{+}\mathbf{R}_{\mathbf{EXPmeas}}\bar{\boldsymbol{\eta}}_{\mathbf{EXP}} \tag{1.37}$$

Or moving everything to the left had side gives

$$\mathbf{R}_{\mathbf{TS}}^{+}\mathbf{R}_{\mathbf{FEmeas}}\bar{\boldsymbol{\eta}}_{\mathbf{FE}} - \mathbf{R}_{\mathbf{TS}}^{+}\mathbf{R}_{\mathbf{EXPmeas}}\bar{\boldsymbol{\eta}}_{\mathbf{EXP}} = \mathbf{0}. \tag{1.38}$$

A similar process can be applied to the second constraint of (1.36). The constraints can now be written in the form given in (1.12)–(1.14) as

$$\begin{bmatrix} \mathbf{R}_{\mathbf{TS}}^{+} & 0 \\ 0 & \mathbf{R}_{\mathbf{TS}}^{+} \end{bmatrix} \begin{bmatrix} \mathbf{I} & -\mathbf{I} & \mathbf{0} \\ \mathbf{0} & \mathbf{I} & -\mathbf{I} \end{bmatrix} \begin{bmatrix} \mathbf{R}_{\mathbf{FEmeas}} & \mathbf{0} & \mathbf{0} \\ \mathbf{0} & \mathbf{R}_{\mathbf{EXPmeas}} & \mathbf{0} \\ \mathbf{0} & \mathbf{0} & \mathbf{R}_{\mathbf{TS}} \end{bmatrix} \begin{Bmatrix} \boldsymbol{\eta}_{\mathbf{FE}} \\ \boldsymbol{\eta}_{\mathbf{EXP}} \\ \boldsymbol{\eta}_{\mathbf{TS}} \end{Bmatrix} = \begin{Bmatrix} 0 \\ 0 \end{Bmatrix} \tag{1.39}$$

Where Ψ_c^{BD+}in (1.11) is $\mathbf{R}_{TS}^{BD+}$ and $\mathbf{B}$ is the Boolean matrix here, thus

$$\tilde{\mathbf{B}} = \begin{bmatrix} \mathbf{R}_{\mathbf{TS}}^{+} & 0 \\ 0 & \mathbf{R}_{\mathbf{TS}}^{+} \end{bmatrix} \begin{bmatrix} \mathbf{I} & -\mathbf{I} & \mathbf{0} \\ \mathbf{0} & \mathbf{I} & -\mathbf{I} \end{bmatrix} \begin{bmatrix} \mathbf{R}_{\mathbf{FEmeas}} & \mathbf{0} & \mathbf{0} \\ \mathbf{0} & \mathbf{R}_{\mathbf{EXPmeas}} & \mathbf{0} \\ \mathbf{0} & \mathbf{0} & \mathbf{R}_{\mathbf{TS}} \end{bmatrix}. \tag{1.40}$$

Repeating (1.17) and (1.18) here for clarity gives

$$\bar{\boldsymbol{\eta}} = \tilde{\mathbf{L}}\bar{\boldsymbol{\varepsilon}} \tag{1.41}$$

and

$$\tilde{\mathbf{B}}\tilde{\mathbf{L}}\bar{\boldsymbol{\varepsilon}} = \bar{\mathbf{0}} \tag{1.42}$$

and $\tilde{\mathbf{L}}$is the null space of $\tilde{\mathbf{B}}$,which is known. Substitute (1.41) into (1.34) and premultiply by $\tilde{\mathbf{L}}^T$ to give

$$\mathbf{L}^T \begin{bmatrix} \boldsymbol{\omega}_{\mathbf{FE}}^2 & \mathbf{0} & \mathbf{0} \\ \mathbf{0} & \boldsymbol{\omega}_{\mathbf{EXP}}^2 & \mathbf{0} \\ \mathbf{0} & \mathbf{0} & -2\boldsymbol{\omega}_{\mathbf{TS}}^2 \end{bmatrix} \mathbf{L}\bar{\boldsymbol{\varepsilon}} - \boldsymbol{\omega}^2 \mathbf{L}^T \begin{bmatrix} \mathbf{I}_{\mathbf{FE}} & \mathbf{0} & \mathbf{0} \\ \mathbf{0} & \mathbf{I}_{\mathbf{EXP}} & \mathbf{0} \\ \mathbf{0} & \mathbf{0} & -2\mathbf{I}_{\mathbf{TS}} \end{bmatrix} \mathbf{L}\ddot{\bar{\boldsymbol{\varepsilon}}} = \bar{0} \tag{1.43}$$

providing the coupled equations from which the eigenvalue problem can be solved yielding. The solution will provide a set of eigenvectors, Φ, frequencies, $\boldsymbol{\omega}^2$, and modal coordinates, $\bar{\boldsymbol{\beta}}$. Now the coupled displacements will be

$$\bar{\mathbf{y}} = \mathbf{RL}\Phi\bar{\boldsymbol{\beta}}. \tag{1.44}$$

The resulting new damping matrix is formed by

$$\Phi^T \mathbf{L}^T \begin{bmatrix} \boldsymbol{\omega}_{\mathbf{FE}}^2 & \mathbf{0} & \mathbf{0} \\ \mathbf{0} & \boldsymbol{\omega}_{\mathbf{EXP}}^2 & \mathbf{0} \\ \mathbf{0} & \mathbf{0} & -2\boldsymbol{\omega}_{\mathbf{TS}}^2 \end{bmatrix} \mathbf{L}\Phi \tag{1.45}$$

From which we usually just take the diagonal values to give $2\bar{\boldsymbol{\zeta}}_{new_i} * \bar{\boldsymbol{\omega}}_{new_i}$.

1.5 Example Combining Experimental Plate/Beam Substructure with Analytical Cylinder Substructure Using the CMS Approach

Generally, the author does not execute (1.33) in a single step, since it makes the matrices very large and the resulting inversions are computationally too intensive. For this example, assume we have one step where systems C and D in the figure are too be joined. (Another step can be taken to subtract the transmission simulators, which will not be done here). Define **HC** and **HD** as the frequency response function matrices for substructures C and D respectively. **HT** is the FRF matrix of the total system after C and D are coupled. Each substructure has a two dimensional FRF matrix for every frequency line of the FRFs. The first subscript on any of these matrices represents the output response dof and the second subscript represents the input force dof. Perhaps the two most useful equations from partitions of the classical method in (1.29) are

$$\mathbf{HT}_{ri} = \mathbf{HD}_{rc}(\mathbf{HD}_{cc} + \mathbf{HC}_{cc})^{-1}\mathbf{HC}_{ci} \tag{1.46}$$

where the force input is on substructure C and the response output is on substructure D, and

$$\mathbf{HT}_{ri} = \mathbf{HC}_{ri} - \mathbf{HC}_{rc}(\mathbf{HD}_{cc} + \mathbf{HC}_{cc})^{-1}\mathbf{HC}_{ci} \tag{1.47}$$

where the force input is on substructure C and the response output is also on substructure C. Here the subscript *r* represents the output response and the subscript *i* represents the input force, and the subscript *c* represents the connection dof between

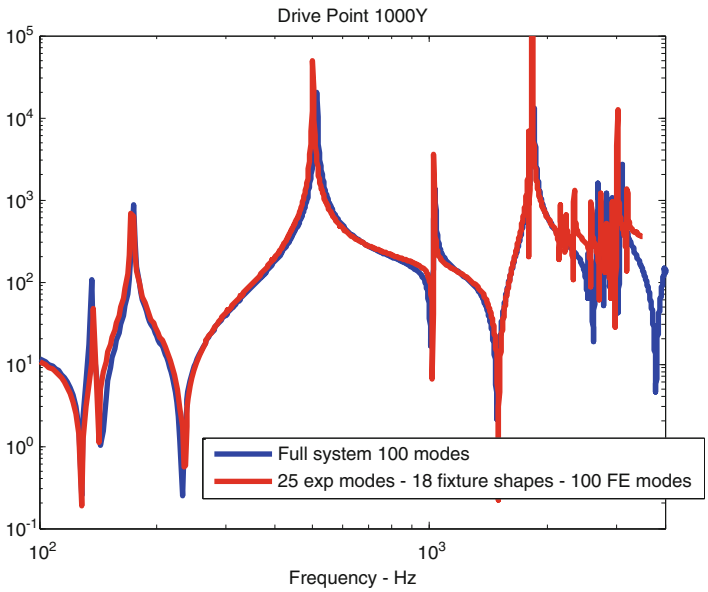

Fig. 1.4 Transmission simulator method FRF of coupled system (*red*) versus truth model (*blue*) – Driving point response at tip of beam in Fig. 1.1 (color figure online)

the two substructures. With the transmission simulator method, the Boolean matrix $\mathbf{B}$ is replaced with $\hat{\mathbf{B}}$ to convert all the connection dof to modal dof of the transmission simulator in (1.33), so that

$$\mathbf{HD}_{rc} = \mathbf{HD}_{rp}\mathbf{R}_{TS}^{T+} \tag{1.48}$$

$$\mathbf{HD}_{cc} = \mathbf{R}_{TS}^{+}\mathbf{HD}_{pp}\mathbf{R}_{TS}^{T+} \tag{1.49}$$

$$\mathbf{HC}_{cc} = \mathbf{R}_{TS}^{+}\mathbf{HC}_{pp}\mathbf{R}_{TS}^{T+} \tag{1.50}$$

$$\mathbf{HC}_{ci} = \mathbf{R}_{TS}^{+}\mathbf{HC}_{pi} \tag{1.51}$$

$$\mathbf{HC}_{rc} = \mathbf{HC}_{rp}\mathbf{R}_{TS}^{T+} \tag{1.52}$$

in (1.46) and (1.47). The subscript p represents the dof at the transmission simulator measurement locations on either substructure. The pseudo-inverse of the mode shape matrix $\mathbf{R}_{TS}$ of the transmission simulator reduces the size of the physical measurement FRF matrices down to the number of modes kept for the transmission simulator at all the connection dof.

In Fig. 1.4 one can see the axial FRF at the tip of the beam (see Fig. 1.1 for location). The red FRF was constructed from the modal parameters of the coupled system mode shapes, frequencies and damping using the transmission simulator method with the CMS approach. The blue FRF represents the truth data constructed from the modal parameters of a highly validated finite element model of the full system.

References

1. Allen MS, Mayes RL (2007) Comparison of FRF and modal methods for combining experimental and analytical substructures. In: Proceedings of the 25th IMAC conference on structural dynamics, Paper #269, Orlando
2. Mayes RL, Stasiunas EC (2007) Combining lightly damped experimental substructures with analytical substructures. In: Proceedings of the 25th IMAC conference on structural dynamics, Paper #207, Orlando
3. Mayes RL, Allen MS, Kammer DC (2012) Eliminating indefinite mass matrices with the transmission simulator method of substructuring. In: Proceedings of the 30th IMAC Conference on Structural Dynamics, Paper #163, Jacksonville, FL
4. de Klerk D, Rixen DJ, Voormeeren SN (2008) General framework for dynamic substructuring: history, review, and classification of techniques. AIAA J 46(5):1169–1181

Chapter 2
Experimental–Analytical Substructure Model Sensitivity Analysis for Cutting Machine Chatter Prediction

Anders Liljerehn and Thomas Abrahamsson

Abstract Process reliability and dynamic stability is a growing customer demand in the metal machining industry. A limiting factor in process stability is regenerative vibrations which may damage the machined component, the cutting tool and even the machine tool. Spindle speed optimization to ensure process stability and enable larger cutting depths is based on the machine tool and cutting tool assembly's frequency response at the tool-tip. The traditional procedure to retrieve the tool-tip frequency response is to conduct dynamic testing of each machine tool mounted cutting tool. This methodology is normally very time-consuming. In an attempt to reduce testing time, receptance coupling substructure analysis (RCSA) has been proposed by a number of researchers. The objective with this approach is to measure the machine tool structure once and then couple a finite element based substructure representation of the cutting tool of interest. The accuracy of the predicted tool-tip frequency response is then dependent on the quality of measured data. This paper details the state-space based sub-structure coupling technique that is used and presents a sensitivity analysis. This analysis distinguishes key considerations for the machine tool component test and it quantifies the parameter influence on the process stability predictions of the coupled system.

2.1 Introduction

In metal cutting, spindle speed optimization for process stability is one example of action that may reduce production time and increase process reliability. For process stability, it is crucial to avoid regenerative vibrations due to feedback of the cutting forces and thereby enable larger cutting depth, with higher material removal rate as benefit. An analytical spindle speed optimization is based on the real part of frequency response functions, FRFs, in two orthogonal transversal directions at the tool tip of a machine tool and cutting tool assembly. Based on the real part of the tool tip FRFs a chart of what is known as stability lobes can be constructed see Fig. 2.1. The stability lobe chart indicates optimal spindle speeds where regenerative vibrations can be avoided for larger depths of cut. The chart, Fig. 2.1, should be read as follows. A stable machining process can be expected if the spindle speed and axial depth of cut is in a combined state in the stable region of the chart. In the unstable state, however, regenerative vibrations also known as chatter do occur. From the stability chart one can see that some spindle speeds are more beneficial than others where greater cutting depths, and thus a better production, are allowed without encountering chatter.

The stability chart is only constructed out of the negative values of the real FRF in two orthogonal main directions at the tool tip of the cutting tool. The creation of the whole set of stability lobes to create the complete stability chart is based on the phase shifts between the vibration marks left on the machined surface made from one cutting tooth to the next tooth that comes in to cut, see [1].

Stability lobe predictions have been a vast research area since the early 1960s, [2, 3]. One of the limitations of FRF-based chatter predictions is that the FRF at the tool tip of a machine tool and cutting tool assembly only yields for a specific setup.

A. Liljerehn (✉)
AB Sandvik Coromant, R & D Metal Cutting Research, Sandviken SE-811 81, Sweden
e-mail: anders.c.liljerehn@sandvik.com

T. Abrahamsson
Dept Applied Mechanics, Chalmers University of Technology, Gothenburg SE-41296, Sweden
e-mail: thomas.abrahamsson@chalmers.se

R.L. Mayes et al. (eds.), *Topics in Experimental Dynamics Substructuring and Wind Turbine Dynamics, Volume 2*,
Conference Proceedings of the Society for Experimental Mechanics Series 27,
DOI 10.1007/978-1-4614-2422-2_2,

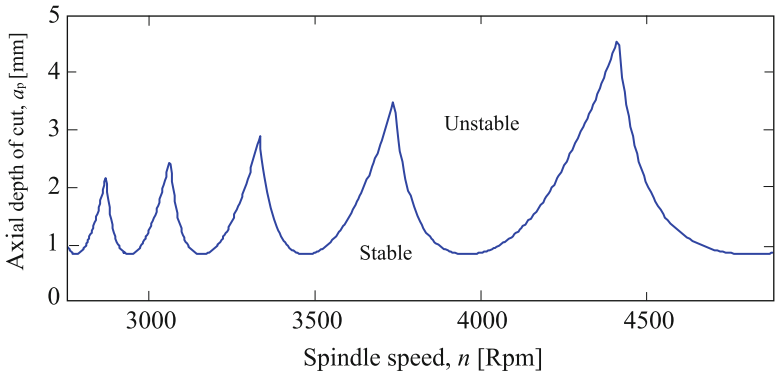

Fig. 2.1 Stability lobe chart

Larger production plants are usually equipped with a substantial amount of cutting tools in their machine tools. To measure each cutting tool combination is not only time consuming but it also requires that the machine tool is taken out of operation during measurements. This results in productivity losses which in many cases are regarded as unacceptable by the plant company. To reduce testing time receptance coupling substructure analysis (RCSA) has been utilized by a number of researchers. The objective with this approach is to only measure the machine tool structure once and then couple a substructure representation of the cutting tool of interest into an assembly.

To use a receptance coupling technique by synthesizing the frequency response displacement function of the system is indeed very appealing but is not without obstacles. This paper is a factor relevance investigation, trying to answer questions that aroused after the writing of [4]. One of the conclusions drawn in [4] was that a slight overestimation of the first bending mode of the coupled system's spindle/cutting tool assembly, compared to verification measurements, can have a large impact on the stability chart. The question of which parameters effects the result of the substructured system is one of the key understandings that need to be in place in order to conduct relevant measurements and stability lobe predictions.

The factor relevance investigation in this paper is strictly restricted to FRFs generated from FEM of the assembly components. The models are described in [4] and the coupling routines used are fully described in [5]. The approach of using synthetic data has been chosen in order to avoid the complexity and uncertainties that follows with measurements in terms of noise, misalignment of force and output sensors, etc. The necessity of further sensitivity analyses to the measurement problem is evident but excluded from this paper.

2.2 Component Synthesis

Component substructuring is usually divided in to two main categories. The first is direct frequency response function coupling [6–11]. The direct FRF coupling method has the advantage that it is fast in that sense that it can be applied directly on measured FRFs and don't require a system identification data processing. The absence of data processing is also its biggest disadvantage since it makes this type of coupling techniques sensitive to noise. The other type of coupling methods often found in literature is component mode synthesis [12–15]. This method has the advantage that it diminishes the noise problems but on the other hand requires that the mode shapes are captured well and it may also suffer from errors that can come from mode truncation. The mode truncation issue for the modal synthesis coupling technique is not a problem in the direct FRF coupling methods since the influences of higher frequency modes are accounted for in the measurement data. The component synthesis used in this sensitivity analysis is based on the state-space coupling method proposed in [5]. This coupling method utilizes the benefits of noise suppression introduced by modal analysis. This is done by coupling of identified first-order state-space substructure component models. The coupling method is used to couple two subsystems ($i = 1, 2$) on state-space form with displacement or velocities as output. A state-space model with external force inputs $\mathbf{u}$ and displacement outputs $\mathbf{y}$ can be written as follows

$$\begin{cases} \dot{\mathbf{x}}^i = \mathbf{A}^i\mathbf{x}^i + \mathbf{B}^i\mathbf{u}^i \\ \mathbf{y}^i = \mathbf{C}^i\mathbf{x}^i \end{cases} \tag{2.1}$$

The state vector is $\mathbf{x}$, and $\mathbf{A}$, $\mathbf{B}$ and $\mathbf{C}$ are constant coefficient matrices. Both subsystems are partitioned with respect to coupling degrees of freedom (DOFs), subscript c, and other DOFs, subscript o, according to the partition of response and loading

$$\mathbf{y}^i = \begin{Bmatrix} \mathbf{y}_c{}^i \\ \mathbf{y}_o{}^i \end{Bmatrix} \quad \mathbf{u}^i = \begin{Bmatrix} \mathbf{u}_c{}^i \\ \mathbf{u}_o{}^i \end{Bmatrix} \tag{2.2}$$

Using the non-uniqueness of state-space representations, the system might be transformed with similarity transformation without approximation. A similarity transform $\mathbf{T}$ with certain properties transforms the states as

$$\tilde{\mathbf{x}}^i = \mathbf{T}^i \mathbf{x}^i = \begin{Bmatrix} \dot{\mathbf{y}}_c{}^i \\ \mathbf{y}_c{}^i \\ \mathbf{x}_o{}^i \end{Bmatrix} \tag{2.3}$$

it can be shown, see [5], that the state-space matrices in this case turn into the particular coupling form as

$$\tilde{\mathbf{A}}^i = \begin{bmatrix} \mathbf{A}^i_{vv} & \mathbf{A}^i_{vd} & \mathbf{A}^i_{vo} \\ \mathbf{I} & \mathbf{0} & \mathbf{0} \\ \mathbf{0} & \mathbf{A}^i_{od} & \mathbf{A}^i_{oo} \end{bmatrix} \quad \tilde{\mathbf{B}}^i = \begin{bmatrix} \mathbf{B}^i_{vv} & \mathbf{B}^i_{vo} \\ \mathbf{0} & \mathbf{0} \\ \mathbf{0} & \mathbf{B}^i_{oo} \end{bmatrix} \quad \tilde{\mathbf{C}}^i = \begin{bmatrix} \mathbf{0} & \mathbf{I} & \mathbf{0} \\ \mathbf{C}^i_{ov} & \mathbf{C}^i_{od} & \mathbf{C}^i_{oo} \end{bmatrix} \tag{2.4}$$

The partition subscripts indicate velocity outputs (v), displacement outputs (d) and other states (o), all in accordance with (2.3). The next stage in order to couple the models together, equilibrium and compatibility conditions has to be taken in to account at the coupling DOFs. For response and excitation of two subsystems that are co-oriented and numbered in the same order we can write the relation between the response and the excitation quantities between the uncoupled subsystem models and the synthesized models as

$$\begin{Bmatrix} \mathbf{y}^I_c \\ \mathbf{y}^{II}_c \end{Bmatrix} = \begin{bmatrix} \mathbf{I} \\ \mathbf{I} \end{bmatrix} \bar{\mathbf{y}}_c \quad \bar{\mathbf{u}}_c = \begin{bmatrix} \mathrm{I} & \mathrm{I} \end{bmatrix} \begin{Bmatrix} \mathbf{u}^{\mathrm{I}}_c \\ \mathbf{u}^{\mathrm{II}}_c \end{Bmatrix} \tag{2.5}$$

and from here on considering coupling responses only in displacement, $\mathbf{y}_c{}^i$ for simplicity. We can now write the state-space realization on coupled form using (2.4) and (2.5), which is defined as

$$\begin{Bmatrix} \ddot{\bar{\mathbf{y}}}_c \\ \dot{\bar{\mathbf{y}}}_c \\ \dot{\mathbf{x}}_o \end{Bmatrix} = \begin{bmatrix} \mathbf{A}^i_{vv} & \mathbf{A}^i_{vd} & \mathbf{A}^i_{vo} \\ \mathbf{I} & \mathbf{0} & \mathbf{0} \\ \mathbf{0} & \mathbf{A}^i_{od} & \mathbf{A}^i_{oo} \end{bmatrix} \begin{Bmatrix} \dot{\bar{\mathbf{y}}}_c \\ \bar{\mathbf{y}}_c \\ \mathbf{x}_o \end{Bmatrix} + \begin{bmatrix} \mathbf{B}^i_{vv} & \mathbf{B}^i_{vo} \\ \mathbf{0} & \mathbf{0} \\ \mathbf{0} & \mathbf{B}^i_{oo} \end{bmatrix} \begin{Bmatrix} \bar{\mathbf{u}}_c \\ \mathbf{u}_o \end{Bmatrix} \tag{2.6a}$$

$$\begin{Bmatrix} \bar{\mathbf{y}}_c \\ \mathbf{y}_o \end{Bmatrix} = \begin{bmatrix} \mathbf{0} & \mathbf{I} & \mathbf{0} \\ \mathbf{C}^i_{ov} & \mathbf{C}^i_{od} & \mathbf{C}^i_{oo} \end{bmatrix} \begin{Bmatrix} \dot{\bar{\mathbf{y}}}_c \\ \bar{\mathbf{y}}_c \\ \mathbf{x}_o \end{Bmatrix} \tag{2.6b}$$

The advantage of using first-order state-space models in lieu to a second-order modal model is that the state-space model has lesser restriction which enables this model to better reproduce the measured data. However, some physical properties, introduced as constraints in the system identification phase, have been found to enhance the first-order state-space model, [5]. To enforce these kinematic and equilibrium constraints we first need to transform the two subcomponents, subsystem I and subsystem II, in to coupling form in accordance with (2.6a) and (2.6b). The first kinematic constraint to enforce is that the interface velocities and displacements should be equal. This is done by considering the first row of equation (2.6a) from which we have that the acceleration output for substructure I, 2.7a and II, 2.7b can be formulated as

$$\ddot{\bar{\mathbf{y}}}^I_c = \mathbf{A}^I_{vv} \dot{\bar{\mathbf{y}}}^I_c + \mathbf{A}^I_{vd} \bar{\mathbf{y}}^I_c + \mathbf{A}^I_{vo} \mathbf{x}^I_o + \mathbf{B}^I_{vv} \bar{\mathbf{u}}^I_c + \mathbf{B}^I_{vo} \mathbf{u}^I_o \tag{2.7a}$$

$$\ddot{\bar{\mathbf{y}}}^{II}_c = \mathbf{A}^{II}_{vv} \dot{\bar{\mathbf{y}}}^{II}_c + \mathbf{A}^{II}_{vd} \bar{\mathbf{y}}^{II}_c + \mathbf{A}^{II}_{vo} \mathbf{x}^{II}_o + \mathbf{B}^{II}_{vv} \bar{\mathbf{u}}^{II}_c + \mathbf{B}^{II}_{vo} \mathbf{u}^{II}_o \tag{2.7b}$$

and to fulfill the stated kinematic constraints it follows that the velocity output at the coupling DOFs, 2.8a, satisfies

$$\dot{\bar{\mathbf{y}}}_{\mathrm{c}}^{I} = \dot{\bar{\mathbf{y}}}_{\mathrm{c}}^{II} \overset{def}{=} \dot{\bar{\mathbf{y}}}_{\mathrm{c}} \tag{2.8a}$$

and the displacement output at the coupling DOFs 2.8b, satisfies

$$\bar{\mathbf{y}}_{\mathrm{c}}^{I} = \bar{\mathbf{y}}_{\mathrm{c}}^{II} \overset{def}{=} \bar{\mathbf{y}}_{\mathrm{c}} \tag{2.8b}$$

and the equilibrium conditions are met for substructure I, 2.9a and II, 2.9b respectively

$$\bar{\mathbf{u}}_{\mathrm{c}}^{I} = \bar{\mathbf{u}}_{\mathrm{c}}^{I,II} + \bar{\mathbf{u}}_{\mathrm{c,e}}^{I} \tag{2.9a}$$

$$\bar{\mathbf{u}}_{\mathrm{c}}^{II} = -\bar{\mathbf{u}}_{\mathrm{c}}^{I,II} + \bar{\mathbf{u}}_{\mathrm{c,e}}^{II} \tag{2.9b}$$

Where $\bar{\mathbf{u}}_{c}^{I,II}$ denotes the cross-sectional force between the two subsystems and $\bar{\mathbf{u}}_{c,e}$ denotes the externally applied force to the interface DOFs. By introducing (2.8a,b) and (2.9a,b) into (2.7a,b) we get

$$\ddot{\bar{\mathbf{y}}}_{\mathrm{c}} = \mathbf{A}_{\mathrm{vv}}^{I}\dot{\bar{\mathbf{y}}}_{\mathrm{c}} + \mathbf{A}_{\mathrm{vd}}^{I}\bar{\mathbf{y}}_{\mathrm{c}} + \mathbf{A}_{\mathrm{vo}}^{I}\mathbf{x}_{\mathrm{o}}^{I} + \mathbf{B}_{\mathrm{vv}}^{I}\bar{\mathbf{u}}_{\mathrm{c}}^{I,II} + \mathbf{B}_{\mathrm{vv}}^{I}\bar{\mathbf{u}}_{\mathrm{c,e}}^{I} + \mathbf{B}_{\mathrm{vo}}^{I}\mathbf{u}_{\mathrm{o}}^{I} \tag{2.10a}$$

$$\ddot{\bar{\mathbf{y}}}_{\mathrm{c}} = \mathbf{A}_{\mathrm{vv}}^{II}\dot{\bar{\mathbf{y}}}_{\mathrm{c}} + \mathbf{A}_{\mathrm{vd}}^{II}\bar{\mathbf{y}}_{\mathrm{c}} + \mathbf{A}_{\mathrm{vo}}^{II}\mathbf{x}_{\mathrm{o}}^{II} - \mathbf{B}_{\mathrm{vv}}^{II}\bar{\mathbf{u}}_{\mathrm{c}}^{I,II} + \mathbf{B}_{\mathrm{vv}}^{II}\bar{\mathbf{u}}_{\mathrm{c,e}}^{II} + \mathbf{B}_{\mathrm{vo}}^{II}\mathbf{u}_{\mathrm{o}}^{II} \tag{2.10b}$$

The mass inertial of the interface DOFs correspond to the inverse of $\mathbf{B}_{vv}^{I}$ and $\mathbf{B}_{vv}^{II}$. To introduce these kinematic constraints the first step is to multiply (2.10a) with $\left(\mathbf{B}_{vv}^{I}\right)^{-1}$ from the left and (2.10b) with $\left(\mathbf{B}_{vv}^{II}\right)^{-1}$ also from the left and add them together.

$$\begin{aligned}\left(\left(\mathbf{B}_{\mathrm{vv}}^{I}\right)^{-1} + \left(\mathbf{B}_{\mathrm{vv}}^{II}\right)^{-1}\right)\ddot{\bar{\mathbf{y}}}_{\mathrm{c}} = {} & \left(\left(\mathbf{B}_{\mathrm{vv}}^{I}\right)^{-1}\mathbf{A}_{\mathrm{vv}}^{I} + \left(\mathbf{B}_{\mathrm{vv}}^{II}\right)^{-1}\mathbf{A}_{\mathrm{vv}}^{II}\right)\dot{\bar{\mathbf{y}}}_{\mathrm{c}} \\ & + \left(\left(\mathbf{B}_{\mathrm{vv}}^{I}\right)^{-1}\mathbf{A}_{\mathrm{vd}}^{I} + \left(\mathbf{B}_{\mathrm{vv}}^{II}\right)^{-1}\mathbf{A}_{\mathrm{vd}}^{II}\right)\bar{\mathbf{y}}_{\mathrm{c}} \\ & + \left(\mathbf{B}_{\mathrm{vv}}^{I}\right)^{-1}\mathbf{A}_{\mathrm{vo}}^{I}\mathbf{x}_{\mathrm{o}}^{I} + \left(\mathbf{B}_{\mathrm{vv}}^{II}\right)^{-1}\mathbf{A}_{\mathrm{vo}}^{II}\mathbf{x}_{\mathrm{o}}^{II} + \bar{\mathbf{u}}_{\mathrm{c}} \\ & + \left(\mathbf{B}_{\mathrm{vv}}^{I}\right)^{-1}\mathbf{B}_{\mathrm{vo}}^{I}\mathbf{u}_{\mathrm{o}}^{II} + \left(\mathbf{B}_{\mathrm{vv}}^{II}\right)^{-1}\mathbf{B}_{\mathrm{vo}}^{II}\mathbf{u}_{\mathrm{o}}^{II}\end{aligned} \tag{2.11}$$

were $\bar{\mathbf{u}}_{\mathrm{c}}$is the total external load applied to assembled components interface DOFs and is defined as

$$\bar{\mathbf{u}}_{\mathrm{c}} \overset{def}{=} \bar{\mathbf{u}}_{\mathrm{c}}^{I} + \bar{\mathbf{u}}_{\mathrm{c}}^{II} = \bar{\mathbf{u}}_{\mathrm{c}}^{I,II} + \bar{\mathbf{u}}_{\mathrm{c,e}}^{I} - \bar{\mathbf{u}}_{\mathrm{c}}^{I,II} + \bar{\mathbf{u}}_{\mathrm{c,e}}^{II} = \bar{\mathbf{u}}_{\mathrm{c,e}}^{I} + \bar{\mathbf{u}}_{\mathrm{c,e}}^{II} \tag{2.12}$$

rearranging (2.11) slightly we can write it in the following structure

$$\ddot{\bar{\mathbf{y}}}_{\mathrm{c}} = \bar{\mathbf{A}}_{\mathrm{vv}}\dot{\bar{\mathbf{y}}}_{\mathrm{c}} + \bar{\mathbf{A}}_{\mathrm{vd}}\bar{\mathbf{y}}_{\mathrm{c}} + \bar{\mathbf{A}}_{\mathrm{vo}}^{I}\mathbf{x}_{\mathrm{o}}^{I} + \bar{\mathbf{A}}_{\mathrm{vo}}^{II}\mathbf{x}_{\mathrm{o}}^{II} + \bar{\mathbf{B}}_{\mathrm{vv}}\bar{\mathbf{u}}_{\mathrm{c}}^{II} + \mathbf{B}_{\mathrm{vo}}^{I}\bar{\mathbf{u}}_{\mathrm{o}}^{I} + \mathbf{B}_{\mathrm{vo}}^{II}\bar{\mathbf{u}}_{\mathrm{o}}^{II} \tag{2.13}$$

where

$$\bar{\mathbf{A}}_{\mathrm{vv}} = \mathbf{B}_{\mathrm{vv}}^{II}\left(\mathbf{B}_{\mathrm{vv}}^{I} + \mathbf{B}_{\mathrm{vv}}^{II}\right)^{-1}\mathbf{A}_{\mathrm{vv}}^{I} + \mathbf{B}_{\mathrm{vv}}^{I}\left(\mathbf{B}_{\mathrm{vv}}^{I} + \mathbf{B}_{\mathrm{vv}}^{II}\right)^{-1}\mathbf{A}_{\mathrm{vv}}^{II} \tag{2.14}$$

$$\bar{\mathbf{A}}_{\mathrm{vd}} = \mathbf{B}_{\mathrm{vv}}^{II}\left(\mathbf{B}_{\mathrm{vv}}^{I} + \mathbf{B}_{\mathrm{vv}}^{II}\right)^{-1}\mathbf{A}_{\mathrm{vd}}^{I} + \mathbf{B}_{\mathrm{vv}}^{I}\left(\mathbf{B}_{\mathrm{vv}}^{I} + \mathbf{B}_{\mathrm{vv}}^{II}\right)^{-1}\mathbf{A}_{\mathrm{vd}}^{II} \tag{2.15}$$

$$\bar{\mathbf{A}}_{\mathrm{vo}}^{I} = \mathbf{B}_{\mathrm{vv}}^{II}\left(\mathbf{B}_{\mathrm{vv}}^{I} + \mathbf{B}_{\mathrm{vv}}^{II}\right)^{-1}\mathbf{A}_{\mathrm{vo}}^{I} \tag{2.16}$$

$$\bar{\mathbf{A}}_{\mathrm{vo}}^{II} = \mathbf{B}_{\mathrm{vv}}^{I}\left(\mathbf{B}_{\mathrm{vv}}^{I} + \mathbf{B}_{\mathrm{vv}}^{II}\right)^{-1}\mathbf{A}_{\mathrm{vo}}^{II} \tag{2.17}$$

$$\bar{\mathbf{B}}_{\mathrm{vv}} = \mathbf{B}_{\mathrm{vv}}^{I}\left(\mathbf{B}_{\mathrm{vv}}^{I} + \mathbf{B}_{\mathrm{vv}}^{II}\right)^{-1}\mathbf{B}_{\mathrm{vv}}^{II} \tag{2.18}$$

$$\bar{\mathbf{B}}^{I}_{\mathrm{vo}} = \mathbf{B}^{II}_{\mathrm{vv}}\left(\mathbf{B}^{I}_{\mathrm{vv}} + \mathbf{B}^{II}_{\mathrm{vv}}\right)^{-1}\mathbf{B}^{I}_{\mathrm{vv}} \tag{2.19}$$

$$\bar{\mathbf{B}}^{II}_{\mathrm{vo}} = \mathbf{B}^{I}_{\mathrm{vv}}\left(\mathbf{B}^{I}_{\mathrm{vv}} + \mathbf{B}^{II}_{\mathrm{vv}}\right)^{-1}\mathbf{B}^{II}_{\mathrm{vv}} \tag{2.20}$$

the assembled systems on state-space form can now be written as

$$\begin{Bmatrix} \ddot{\bar{\mathbf{y}}}_{\mathrm{c}} \\ \dot{\bar{\mathbf{y}}}_{\mathrm{c}} \\ \dot{\mathbf{x}}^{I}_{\mathrm{o}} \\ \dot{\mathbf{x}}^{II}_{\mathrm{o}} \end{Bmatrix} = \begin{bmatrix} \bar{\mathbf{A}}_{\mathrm{vv}} & \bar{\mathbf{A}}_{\mathrm{vd}} & \bar{\mathbf{A}}^{I}_{\mathrm{vo}} & \bar{\mathbf{A}}^{II}_{\mathrm{vo}} \\ \mathbf{I} & 0 & 0 & 0 \\ 0 & \mathbf{A}^{I}_{\mathrm{od}} & \mathbf{A}^{I}_{\mathrm{oo}} & 0 \\ 0 & \mathbf{A}^{II}_{\mathrm{od}} & 0 & \mathbf{A}^{II}_{\mathrm{oo}} \end{bmatrix} \begin{Bmatrix} \dot{\bar{\mathbf{y}}}_{\mathrm{c}} \\ \bar{\mathbf{y}}_{\mathrm{c}} \\ \mathbf{x}^{I}_{\mathrm{o}} \\ \mathbf{x}^{II}_{\mathrm{o}} \end{Bmatrix} + \begin{bmatrix} \bar{\mathbf{B}}_{\mathrm{vv}} & \bar{\mathbf{B}}^{I}_{\mathrm{vo}} & \bar{\mathbf{B}}^{II}_{\mathrm{vo}} \\ 0 & 0 & 0 \\ 0 & \bar{\mathbf{B}}^{I}_{\mathrm{oo}} & 0 \\ 0 & 0 & \bar{\mathbf{B}}^{II}_{\mathrm{oo}} \end{bmatrix} \begin{Bmatrix} \bar{\mathbf{u}}_{\mathrm{c}} \\ \bar{\mathbf{u}}^{I}_{\mathrm{o}} \\ \bar{\mathbf{u}}^{II}_{\mathrm{o}} \end{Bmatrix} \tag{2.21}$$

$$\begin{Bmatrix} \bar{\mathbf{y}}_{\mathrm{c}} \\ \mathbf{y}^{I}_{\mathrm{o}} \\ \mathbf{y}^{II}_{\mathrm{o}} \end{Bmatrix} = \begin{bmatrix} 0 & \mathbf{I} & 0 & 0 \\ \mathbf{C}^{I}_{\mathrm{ov}} & \mathbf{C}^{I}_{\mathrm{od}} & \mathbf{C}^{I}_{\mathrm{oo}} & 0 \\ \mathbf{C}^{II}_{\mathrm{ov}} & \mathbf{C}^{II}_{\mathrm{od}} & 0 & \mathbf{C}^{II}_{\mathrm{oo}} \end{bmatrix} \begin{Bmatrix} \dot{\bar{\mathbf{y}}}_{\mathrm{c}} \\ \bar{\mathbf{y}}_{\mathrm{c}} \\ \mathbf{x}^{I}_{\mathrm{o}} \\ \mathbf{x}^{II}_{\mathrm{o}} \end{Bmatrix} \tag{2.22}$$

For the system studied in this paper which is a non-gyroscopic, non-circulatory and passive mechanical system it is expected that Betti's reciprocity principle should apply. To ensure reciprocity the condition $\mathbf{C}^{i}\mathbf{B}^{i} = \mathbf{0}$ has been enforced, in order for the system to be self-adjoint. The state-space models used have also been forced to be stable and passive, see [5].

2.3 System Setup

The purpose of the investigation is to investigate the causal effects different factors have on the tool tip FRF which is the foundation for the stability lobe chart. This approach requires a system which is free from errors, such as noise and model order uncertainties. The system chosen for this investigation is a simplified FE-model of a test rig used in [4], see Fig. 2.2.

The FE-model of the test rig consists of two substructures, Fig. 2.3. The spring suspended metal block with the clamping unit along with the coupling and the tool family generic part of the cutting tool, referred to as the blank, constitutes subsystem I. The tool tip, with a geometry that may vary within the tool family, is considered to be substructure II. Figure 2.4 shows the DOF numbering of the interface. In this study we are particularly interested in motion in the y- and z-directions, DOFs 2 and 3.

Before proceeding with sensitivity analysis we made a validation of the coupling technique. As a reference we obtained frequency response functions of the total system coupled to an entity by ordinary FEM assembly procedures. We see one example in Fig. 2.5. To mimic the system identification procedures for test data we made a system identification of FRFs given by FEM analysis of substructure I. In the frequency range from 0 to 5 kHz it was found that 30 states were sufficient to capture data. In the FE representation 0.5% damping was introduced to all modes.

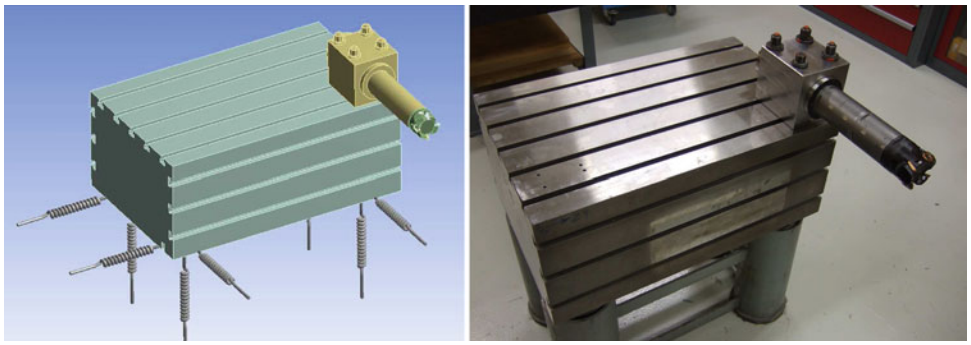

Fig. 2.2 Left; FE-model of test rig. Right; real test rig

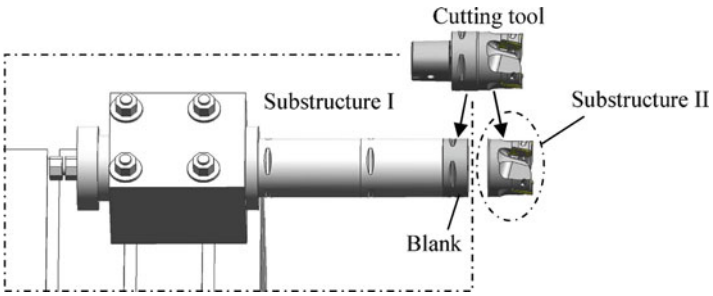

Fig. 2.3 Substructures I and II

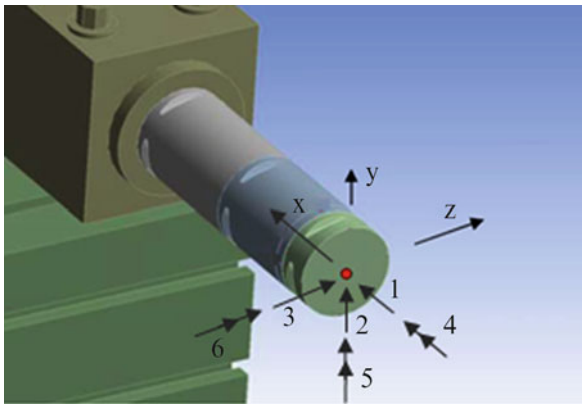

Fig. 2.4 Reference coordinate system and degree of freedom notations

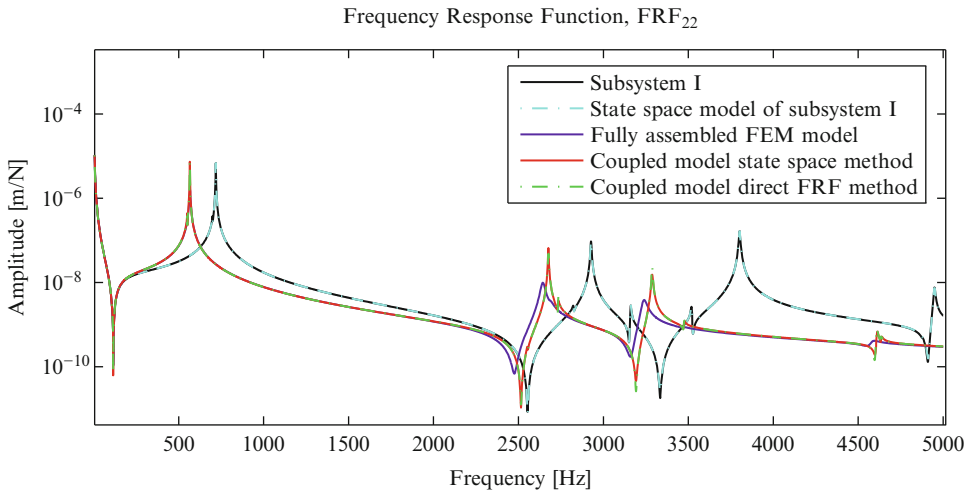

Fig. 2.5 Frequency response function comparison between uncoupled subsystem I and the state space identification of subsystem I as well as the fully assembled FEM model and the assembled substructures using state space and direct FRF coupling technique of the y-direction direct FRF, the FRF_{22}

2.3.1 Results of Validation and Substructuring Method

The result of the state-space coupling of the identified model can be seen in Fig. 2.5. It is seen that it compares favorable to the FEM results and validates the coupling technique. Figure 2.5 also shows the FRF of Subsystem I from FEM and system identification can be seen to match very well. Figure 2.5 also contains and an additional comparison using a direct FRF

coupling method, [6], of the two substructures using generalized frequency domain substructure synthesis. The coupled FRFs using this method match the re-estimated assembled parallel model perfectly which is a good indication that the state space coupling routines works properly. It can be seen in Fig. 2.5 that the FRFs of these three systems matches the fully assembled FEM model very well up and over the first bending mode which is at about 500 Hz. The slight deviation at higher frequencies Is due to model truncation in the synthesis of FRFs of component I.

2.4 Sensitivity Analysis and Evaluation Method

With a reliable identification process in place the next step is the sensitivity analysis based on perturbation of the state space model from modal data and model estimation of that system.

2.4.1 Problem Formulation

The evaluation is limited to investigate the factors governing the accuracy of the predicted spindle speed and depth of cut and *quantify* the impact they have on the predicted stability lobes. A criterion function based on the stability lobe chart is required. The sensitivity analysis is performed through a screening process where each parameter can vary within a certain interval. Each test combination resulted in a perturbed FRF from which a stability lobe chart were obtained. The lobes from the perturbed test were evaluated against a stability lobe chart based on the solution of the unperturbed coupled state space model presented in Fig. 2.5 system based on two criteria.

A first criterion is an evaluation of the angle between stability lobe data vectors of the nominal and perturbed systems. These data vectors are stability lobe functions at discrete spindle speeds. The good thing about this approach is that amplitude of the vectors is disregarded. The angle ranges between 0 and $\pi/2$ were 0 means that the two data vectors are completely parallel and an angle of $\pi/2$ means that the two data vectors are orthogonal. In this evaluation the angle is normalized by taking cosine of the angle resulting in a number ranging from 0 to 1 were 1 means that the two data vectors are perfectly parallel and in that sense equal and 0 means completely orthogonal which is not desirable. We call this normalized angle the co-linearity index

A second evaluation criterion is the minimum axial depth of cut, a_p^{lim}, were the cutting process is stable for all spindle speeds, see Fig. 2.6. This criterion was selected since this depth of cut is the local minimum value of all lobes. This is not the case with the stability peaks which grows with higher spindle speeds. The minimum depth of cut is also the parameter that is especially important when machining at low spindle speeds.

2.4.2 Screening

A traditional screening set up, see [16], is an essential first step of the objective evaluation method that will be used to answer the question of which factors has the largest impact on the criterion function and if there are any interaction between these factors. The aim is to assign all factors the same possibility to influence the criteria and then, if possible, reduce the number

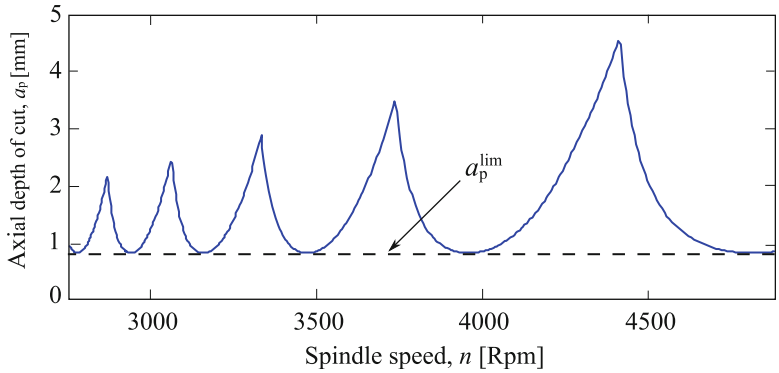

Fig. 2.6 Description of minimum axial depth of cut, a_p^{lim}

Table 2.1 Factors subjected to perturbation in identification of subsystem I

Test nr.	Factor	Change
N1	Number of states that describe first bending mode	Add 2
N2	Number of states that describe first bending mode	Subtract 2
N3	Damping estimation of first bending mode	Add 20%
N4	Damping estimation of first bending mode	Subtract 20%
N5	FRF level	Add 10%
N6	FRF level	Subtract 10%
N7	Cut off frequency for system identification	2 kHz instead of 5 kHz

factors for further investigations. Some of the factors subjected to investigation in this paper have been found to have a strong nonlinear behavior within their range of variation. This makes them unsuitable for the coupled analysis, proposed in [16], which would make it hard to determine their separate impact on the coupled system. A much simpler approach was taken regarding the sensitivity analysis based on the insight that the attempt to investigate the full design space was much to complicate. The approach was instead of changing many parameters all at once to simply change one parameter at the time and keep all others at their reference values. The screening procedure starts with listing, categorizing and determine a relevant range that each factor can vary within. Table 2.1 presents the factors chosen to be investigated in this investigation along with their category and variation span. The screening procedure has multiple objectives. The first is to get an insight of which factors have most influence on the result of the coupled model. If a factor is found to have no influence on the criteria then that result is also useful information. The exclusion of a factor can be proven to be very beneficial from a time or economical perspective. The screening also ranks each factor and therefore gives an indication of which of the factors to put additional focus on.

The chosen factors all contribute differently to the identified models. The number of states included in the state-space model is an interesting parameter to investigate. Previous tests conducted in [17] showed that too few states could influence the coupled systems of but no investigation of the impact of too many states was made. Damping is another parameter of interest since it can normally not be precisely determined from measurements. To see how much amplitude error influences the coupled system is also of interest. This parameter can be influenced from ill calibrated accelerometers, errors in force input measurements and test setup errors. The cut-off frequency will determine how many modes that are taken into account by the state-space substructures and this should influence the coupled system.

2.5 Results

The stability lobe chart is constructed from the real part of FRF_{22} and FRF_{33}, the FRFs associated to transversal motion. Both these directions are important for the final evaluation of the stability lobe chart. The results of a comparison between the real part of the FRF_{22} of the reference and the perturbed systems show how the different parameter influences the location of the bending eigenfrequency and the amplitude of the FRF_{22}, see Fig. 2.7.

Stability lobes for comparison were constructed based on the results of the perturbed FRFs for evaluation. The ingoing cutting parameters used to obtain the stability lobe charts presented in tabled in Table 2.2.

Figure 2.8 shows how the different parameter settings affect the stability lobe chart. It should be noted that the perturbed system with a reduced number of states is not seen in the chosen plot interval. The amplitude of the stability lobes for this setting is much too high to be included in the plot. The drastic impact of this setting is seen in Fig. 2.7.

The plotted stability lobe chart comparison gives a good indication of the influence of different perturbations to the system but it makes it hard to quantify its meaning. The results of the comparisons of the angle between stability lobe data vectors and the minimum value of the depth of cut for each perturbed system compared to the reference system makes it easier to interpret the results. Such results are presented in Table 2.3.

From the results in Table 2.3 it can be seen that the factor with the smallest impact on the system is the one were two additional states has been introduced to add a resonance frequency close to that of the first bending mode. This factor has a very small influence on the angle between the real FRF vectors and almost no influence on the minimum amplitude value compared to the reference. The perturbed system were the state order had been underestimated by neglecting a bending mode showed a significant impact on both evaluation criterions. The damping perturbation proved to have a very small influence on the subspace angle criterion and minimum amplitude seemed to be proportional to the magnitude of the

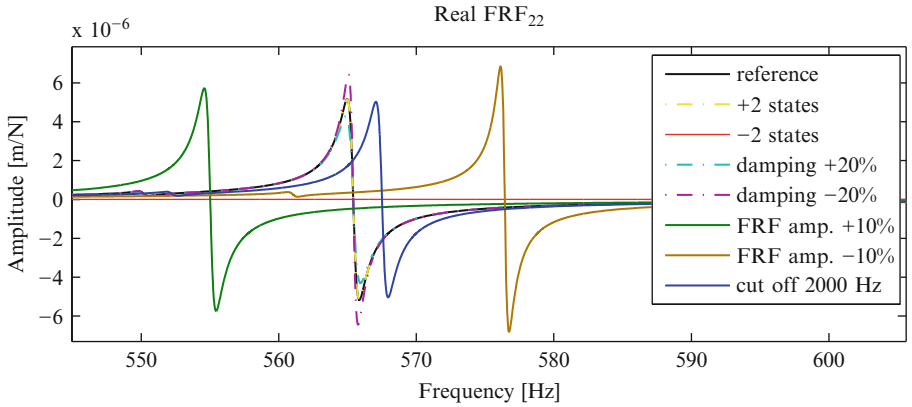

Fig. 2.7 Real part of FRF_{22} of unperturbed (reference) and the perturbed systems

Table 2.2 Cutting parameters used in stability lobe predictions

Cutting parameters	Quantity	Unit
Number of teeth, z	1	–
Tool diameter, D_c	80	[mm]
Radial width of cut, a_e	80	[mm]
Cutting force coefficient in tangential direction, K_t	1319	[MPa]
Cutting force coefficient in radial direction, K_r	789	[MPa]

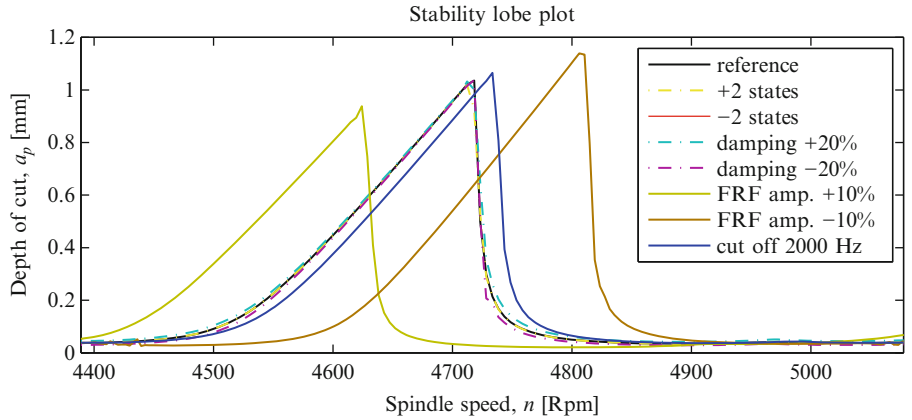

Fig. 2.8 Stability lobe comparisons between unperturbed (reference) and the perturbed systems

Table 2.3 Comparison between the influences of the different perturbation factors minimum axial depth of cut and co-linearity index relative to that of reference configuration

Test nr.	Type of perturbation	Co-linearity index	Minimum axial depth of cut
N1	Number of states +2	0.985	0.99
N2	Number of states −2	0.410	1335.33
N3	Damping estimation of first bending mode +20%	0.975	1.21
N4	Damping estimation of first bending mode −20%	0.976	0.83
N5	FRF amplitude +10%	0.484	0.60
N6	FRF amplitude −10%	0.427	0.81
N7	Cut-off frequency	0.825	1.06

damping. A factor that influenced the coupled system much was the FRF amplitude. The system that had its amplitude increased by 10% underestimated the eigenfrequency with 12 Hz and overestimated the eigenfrequency with 12 Hz with a similar underestimation for an amplitude decrees. Both these errors then propagated to the stability lobe chart resulting in an optimum spindle speed error of 90 rpm. The lowered cut-off frequency perturbation was the fourth least influential perturbation when it comes to the subspace angle criterion. The lowered cut-off frequency also had a small minimum amplitude error.

2.6 Conclusions

The methodology and workflow used to conduct these analyses make up a good foundation for designing the measurement set up. The approach with the two evaluation criteria based on subspace angle and minimum amplitude, makes the evaluation of the perturbed systems much clearer and the two evaluation criteria makes good indications on the comparison to the reference system. This method allows several factors to be evaluated against each other even though they can play a very different role in the identification process. Regarding the results the sensitivity analysis definitely distinguishes the important from the less important parameters. The parameter that influenced the coupled system the most was an error in the estimation of the FRF amplitude. Such significant impact points towards that great care must be taken during the measurement procedure. Accelerometer imprecision of 5% is not uncommon for accelerometers used in these types of measurements. Large accelerometer errors can be expected from temperature transients, calibration errors, linearity errors, frequency and phase response errors, aging errors, cable motion, and electromagnetic interference in cables. Load cell errors affect the FRF estimation similarly. It is seen that the number of states may be very important. This is much in line with the conclusions drawn in [17]. It seems that an excessive state order not necessarily causes bad coupling results as long as the identified modes fit is also shown in the stability chart. The damping perturbation seems to practically only influence the amplitude error in the stability chart. This is good from an application standpoint were the accurate spindle speed is considered much more important than the amplitude of the stability chart. To find the stability limit is fairly easy compared to finding the optimum spindle speed. Regarding the cut-off frequency it is shown that it influences the coupled model but it should not have a large impact as long as no states are disregarded.

References

1. Altintas Y (2000) Manufacturing automation: metal cutting mechanics, machine tool vibrations and CNC design. Cambridge University Press, Cambridge
2. Tlustly J, Polacek M (1963) The Stability of machine tools against self excited vibrations in machining. Int Res Prod Eng ASME 1:465–474
3. Tobias SA (1965) Machine tool vibrations. Blackie and Sons, Glasgow
4. Liljerehn A, Johansson A, Abrahamsson T (2010) Dynamic substructuring in metal cutting machine chatter. In: Proceedings of ISMA2010 international conference on noise and vibration engineering including USD2010, Leuven, 20–22 Sept 2010, ISBN/ISSN: 9789073802872
5. Sjövall P, Abrahamsson T (2007) Component system identification and state-space model synthesis. Mech Syst Signal Process 21(7):2697–2714
6. Jetmundsen B, Bielawa RL, Flanelly G (1988) Generalized frequency domain substructure synthesis. J Am Helicopter Soc 33:55–64
7. Park S, Altintas Y, Movahhedy M (2003) Receptance coupling for end mills. Int J Mach Tools Manu 43:889–896
8. Gordis JH, Bielawa RL, Flannelly WG (1998) A general theory for frequency domain structural synthesis. J Sound Vib 150(1):139–158
9. Liu W, Ewins DJ (2002) Substructure synthesis via elastic media. J Sound Vib 257(2):361–379
10. Lim TC, Li J (2000) A theoretical and computational study of the FRF-based Substructuring technique applying enhanced least square and TSVD approaches. J Sound Vib 231(4):1135–1157
11. Ren Y, Beards CF (1995) On substructure synthesis with FRF data. J Sound Vib 185(5):845–866
12. Craig RR, Bampton MCC (1968) Coupling of substructures for dynamic analysis. AIAA J 6(7):1313–1319
13. Rixen DJ (2004) A dual craig-bampton method for dynamic substructuring. J Comput Appl Math 168:383–391
14. Jen CW, Johanson DA, Dubois F (1995) Numerical modal analysis of structures based on a revised substructure synthesis approach. J Sound Vib 180(2):185–203
15. Balmès E (1996) Use of generalized interface degrees of freedom in component mode synthesis. In: Proceedings of 14th international modal analysis conference, Dearborn
16. Eriksson L, Johansson E, Kettaneh-Wold N, Wikström C, Wold S (2008) Design of experiments: principles and applications. MKS Umetrics AB, Umea 2008
17. Sjövall P, McKelvey T, Abrahamsson T (2006) Constrained state-space system identification with application to structural dynamics. Automatica 42:1539–1546

Chapter 3
Eliminating Indefinite Mass Matrices with the Transmission Simulator Method of Substructuring*

Randy L. Mayes, Mathew S. Allen, and Daniel C. Kammer

Abstract The transmission simulator method of experimental dynamic substructuring captures the interface forces and motions through a fixture called a transmission simulator. The transmission simulator method avoids the need to measure connection point rotations and enriches the modal basis of the substructure model. The free modes of the experimental substructure mounted to the transmission simulator are measured. The finite element model of the transmission simulator is used to couple the experimental substructure to another substructure and to subtract the transmission simulator. However, in several cases the process of subtracting the transmission simulator has introduced an indefinite mass matrix for the experimental substructure. The authors previously developed metrics that could be used to identify which modes of the experimental model led to the indefinite mass matrix. A method is developed that utilizes those metrics with a sensitivity analysis to adjust the transmission simulator mass matrix so that the subtraction does not produce an indefinite mass matrix. A second method produces a positive definite mass matrix by adding a small amount of mass to the indefinite mass matrix. Both analytical and experimental examples are described.

3.1 Introduction

Experimental-analytical substructuring has been a topic of interest since modal testing was first introduced several decades ago. It is appealing because it has the potential to allow one to replace complicated subcomponents with experimental models that may be much less expensive to derive. It also allows the experimentalist to re-use the experimental model, predicting its response in a multitude of other configurations without repeating the test. One can also think of structural modification [1] as a special case of substructuring, where the modification is a special substructure that one wishes to determine in order to produce a desired response, (although the terms "substructuring" and "structural modification" are often used interchangeably [2]).

The authors recently presented a new substructuring methodology, called Modal Constraints for Fixture and Subsystem (MCFS), that has proven quite effective at subtracting one structure from another [3]. Typically one has experimentally measured the modes of a built-up structure and one wishes to remove one subcomponent from that assembly. The subtraction is accomplished by creating a model of the subcomponent that is to be removed, making its mass, stiffness, and damping negative and then coupling the negative subcomponent to the assembly. Whereas, in conventional substructuring one enforces constraints between the points where the substructures are joined, the MCFS method estimates a set of modal

*Sandia is a multiprogram laboratory operated by Sandia Corporation, a Lockheed Martin Company, for the U.S. Department of Energy under Contract DE-AC04-94AL85000.

R.L. Mayes (✉)
Experimental Structural Dynamics, Sandia National Laboratories, Albuquerque, NM, USA
e-mail: rlmayes@sandia.gov

M.S. Allen • D.C. Kammer
Department of Engineering Physics, University of Wisconsin, Madison, WI 53706, USA
e-mail: msallen@engr.wisc.edu; kammer@engr.wisc.edu

R.L. Mayes et al. (eds.), *Topics in Experimental Dynamics Substructuring and Wind Turbine Dynamics, Volume 2*,
Conference Proceedings of the Society for Experimental Mechanics Series 27,
DOI 10.1007/978-1-4614-2422-2_3,

coordinates on the substructure and enforces constraints on those coordinates. This reduces the sensitivity of the method to experimental errors and assures that an appropriate number of constraints is enforced.

The MCFS method is primarily used to estimate a modal model that can be used for substructuring predictions. The substructure is connected to a fixture or transmission simulator [4] and the assembly is tested in free-free conditions. This is equivalent to the well-known method where rigid masses are attached to the structure and used to create a mass-loaded interface, except that the proposed methodology is valid even if the transmission simulator is flexible. The transmission simulator serves to mass-load the interface of the subcomponent, enriching the modal basis and circumventing the need to measure displacements and rotations at the connection point. A model of the transmission simulator is then created and used to subtract its effects from the measured modal model in order to obtain a model for the substructure of interest in isolation, but with an improved modal basis. However, because a system with negative mass has been introduced in order to remove the transmission simulator, the substructure model may not necessarily have a positive definite mass matrix. Similar problems were encountered by other researchers when removing rigid masses from a structure [5]. This paper presents two methods that can be used to assure that the mass matrix of the subcomponent has positive mass.

3.2 Theory

3.2.1 Review of Subtraction of Modal Substructures

Suppose that the natural frequencies, ω_r, damping ratios, ζ_r, and matrix of mass-normalized mode shapes, $\mathbf{\Phi}_{\mathrm{C}}$, of an assembly consisting of the subcomponent of interest and the transmission simulator have been measured. The modal parameters of the transmission simulator are also known. (Here we shall refer to the substructure that is being removed as the transmission simulator, but in a general problem it could be any subcomponent that one wishes to subtract from the assembly). The assembly shall be referred to as system C and the transmission simulator as system A, as in [3], so the uncoupling procedure estimates the modes of B, the component of interest, since $\mathrm{C}-\mathrm{A}=(\mathrm{A}+\mathrm{B})-\mathrm{A}=\mathrm{B}$. First the equations of motion of C and (-A) are concatenated as follows

$$\begin{bmatrix} \mathbf{I}_{\mathrm{C}} & 0 \\ 0 & -\mathbf{I}_{\mathrm{A}} \end{bmatrix} \begin{Bmatrix} \ddot{\mathbf{q}}_{\mathrm{C}} \\ \ddot{\mathbf{q}}_{\mathrm{A}} \end{Bmatrix} + \begin{bmatrix} \left[\backslash 2\zeta_r\omega_r \backslash\right]_{\mathrm{C}} & \mathbf{0} \\ \mathbf{0} & -\left[\backslash 2\zeta_r\omega_r \backslash\right]_{\mathrm{A}} \end{bmatrix} \begin{Bmatrix} \dot{\mathbf{q}}_{\mathrm{C}} \\ \dot{\mathbf{q}}_{\mathrm{A}} \end{Bmatrix} + \begin{bmatrix} \left[\backslash {\omega_r}^2 \backslash\right]_{\mathrm{C}} & \mathbf{0} \\ \mathbf{0} & -\left[\backslash {\omega_r}^2 \backslash\right]_{\mathrm{A}} \end{bmatrix} \begin{Bmatrix} \mathbf{q}_{\mathrm{C}} \\ \mathbf{q}_{\mathrm{A}} \end{Bmatrix} = \begin{Bmatrix} {\mathbf{\Phi}_{\mathrm{C}}}^{\mathrm{T}} \mathbf{F}_{\mathrm{C}} \\ {\mathbf{\Phi}_{\mathrm{A}}}^{\mathrm{T}} \mathbf{F}_{\mathrm{A}} \end{Bmatrix}$$
$$\begin{Bmatrix} \mathbf{y}_{\mathrm{C}} \\ \mathbf{y}_{\mathrm{A}} \end{Bmatrix} = \begin{bmatrix} \mathbf{\Phi}_{\mathrm{C}} & \mathbf{0} \\ \mathbf{0} & \mathbf{\Phi}_{\mathrm{A}} \end{bmatrix} \begin{Bmatrix} \mathbf{q}_{\mathrm{C}} \\ \mathbf{q}_{\mathrm{A}} \end{Bmatrix} \tag{3.1}$$

where the q dof are the generalized modal coordinates of each substructure, and then constraints are enforced as

$$\left[{\mathbf{\Phi}_{\mathrm{A},m}}^{\dagger} \mathbf{\Phi}_{C,m} - \mathbf{I}_{\mathrm{A}} \right] \begin{Bmatrix} \mathbf{q}_{\mathrm{C}} \\ \mathbf{q}_{\mathrm{A}} \end{Bmatrix} = 0 \tag{3.2}$$

Where the superscript, † , denotes the pseudo-inverse of the matrix, and subscript *m* represents degrees of freedom common to both system C and system A that have been measured.

This is done by finding a matrix **B** that transforms the concatenated coordinates into a set of unconstrained coordinates. The coordinates of C are typically a suitable set [6], so one can choose

$$\begin{Bmatrix} \mathbf{q}_{\mathrm{C}} \\ \mathbf{q}_{\mathrm{A}} \end{Bmatrix} = \mathbf{B}\mathbf{q}_{\mathrm{C}}$$
$$\mathbf{B} = \begin{bmatrix} \mathbf{I}_{\mathrm{C}} \\ \boldsymbol{\tau} \end{bmatrix} \tag{3.3}$$

where $\boldsymbol{\tau} = {\mathbf{\Phi}_{\mathrm{A},m}}^{\dagger} \mathbf{\Phi}_{C,m}$. The number of modal coordinates in A and C are denoted N_A and N_C respectively. One can verify that **B** is in the null space of the matrix on the left in (3.2), so these coordinates always satisfy the constraints. As discussed in [3], if the model for the transmission simulator is accurate then the negative transmission simulator model completely